Hindawi
Journal of Combustion
Volume 2018, Article ID 2308419, 13 pages
https://doi.org/10.1155/2018/2308419

*Research Article*

# Growth of Soot Volume Fraction and Aggregate Size in 1D Premixed $C_2H_4$/Air Flames Studied by Laser-Induced Incandescence and Angle-Dependent Light Scattering

**P. N. Langenkamp,[1] J. A. van Oijen,[2] H. B. Levinsky,[1,3] and A. V. Mokhov[1]**

[1]*University of Groningen, Faculty of Science and Engineering, Energy and Sustainability Research Institute Groningen, Nijenborgh 4, 9747 AG Groningen, Netherlands*
[2]*Eindhoven University of Technology, Department of Mechanical Engineering, De Wielen, 5612 AZ Eindhoven, Netherlands*
[3]*DNV GL, Oil & Gas, Energieweg 17, 9743 AN Groningen, Netherlands*

Correspondence should be addressed to A. V. Mokhov; a.v.mokhov@rug.nl

Received 15 June 2018; Accepted 28 August 2018; Published 1 October 2018

Academic Editor: Benjamin Shaw

Copyright © 2018 P. N. Langenkamp et al. This is an open access article distributed under the Creative Commons Attribution License, which permits unrestricted use, distribution, and reproduction in any medium, provided the original work is properly cited.

The growth of soot volume fraction and aggregate size was studied in burner-stabilized premixed $C_2H_4$/air flames with equivalence ratios between 2.0 and 2.35 as function of height above the burner using laser-induced incandescence (LII) to measure soot volume fractions and angle-dependent light scattering (ADLS) to measure corresponding aggregate sizes. Flame temperatures were varied at fixed equivalence ratio by changing the exit velocity of the unburned gas mixture. Temperatures were measured using spontaneous Raman scattering in flames with equivalence ratios up to $\phi = 2.1$, with results showing good correspondence (within 50 K) with temperatures calculated using the San Diego mechanism. Both the soot volume fraction and radius of gyration strongly increase in richer flames. Furthermore, both show a nonmonotonic dependence on flame temperature, with a maximum occurring at ~1675 K for the volume fraction and ~1700 K for the radius of gyration. The measurement results were compared with calculations using two different semiempirical two-equation models of soot formation. Numerical calculations using both mechanisms substantially overpredict the measured soot volume fractions, although the models do better in richer flames. The model accounting for particle coagulation overpredicts the measured radii of gyration substantially for all equivalence ratios, although the calculated values improve at $\phi = 2.35$.

## 1. Introduction

Combustion generated particles such as soot can have a significant impact on combustion equipment, the environment, and human health [1]. This impact is strongly linked to the particles' size and structure. Despite extensive research into this topic, modeling and predicting soot formation and growth in flames remain challenging [2]. Therefore, experimental studies of the formation and growth of soot are indispensable in adding to our understanding of relevant processes and for improving models of soot formation.

To acquire in situ information about soot, laser-induced incandescence (LII) is often used to measure soot volume fractions and sizes of primary particles. Unfortunately, LII cannot provide all the information desired on particle structure, such as particle morphology. Ex situ methods that are often used in conjunction with LII (e.g., transmission electron microscopy, TEM), although relatively easy to interpret and informative, suffer from the drawbacks inherent to invasive sampling, such as perturbation of the reactive flow by the probe and possible incomplete quenching of the particle growth process. Elastic light scattering has been demonstrated to be a suitable noninvasive technique complementing LII to obtain crucial information about soot in flames, such as sizes of primary particles and aggregates [3–5].

Burner-stabilized, premixed 1D flames are particularly suited for testing models of soot formation because they offer well-defined conditions that are readily amenable to analysis.

The properties of these flames are completely determined by the composition and velocity of the unburned fuel/oxidizer mixture, while spatial profiles can be easily remapped to residence times, allowing the study of the dependence of soot formation on temperature and equivalence ratio ($\phi$). Ethylene ($C_2H_4$) is often used as fuel for these studies because 1D ethylene/air flames can be obtained at high $\phi$, where considerable amounts of soot are formed. Soot inception, volume fraction, surface growth, and particle size distribution [6–16] in ethylene flames have been studied extensively using both in situ and ex situ methods. However, since the measured soot volume fractions for premixed flames with identical equivalence ratios show significant variation, even when the measurement techniques are similar [17], it is hard to compare measurements from different studies quantitatively.

The majority of the aforementioned studies did not investigate the effect of flame temperature independently from equivalence ratio; a change in $\phi$ is usually accompanied by a change in flame temperature. Notable exceptions are the studies of Ciajolo et al. [6] and Gu et al. [7] who studied the influence of temperature at fixed $\phi$ on soot volume fraction and particle size distribution, respectively, using physical sampling techniques. To our knowledge, only Böhm et al. [8], Bönig et al. [9], and Chambrion et al. [10] have investigated the influence of flame temperature on soot formation in premixed $C_2H_4$/air flames at constant $\phi$ using noninvasive optical methods. Böhm et al. [8] and Bönig et al. [9] measured the soot volume fraction and particle number density by absorption and scattering techniques. While these parameters determine the total amount of soot in the combustion products, no information on the size and the structure of aggregates, such as the gyration radius and fractal dimension, which are essential for testing models of soot formation, was obtained in these studies. Furthermore, these authors only reported final soot volume fractions, with no information about the time dependence of soot formation in the postflame zone. In addition, to our knowledge, their experimental results have not been compared with model predictions. Meanwhile, Chambrion et al. [10] present only the influence of temperature on the critical C/O ratio at which soot inception starts and on the coagulation rate constant.

In this work we extend the study of Böhm et al. [8] to include the information on the time-dependent soot particle growth and agglomeration by measuring axial profiles of the soot volume fraction, $f_v$, and radius of gyration, $R_g$, and also by comparing them with the results of numerical simulations. Towards this end, we performed measurements for a range of flame conditions using an experimental setup in which flame temperature and equivalence ratio $\phi$ were controlled independently of each other. The experiments were performed in premixed $C_2H_4$/air flames at equivalence ratios $\phi$ in the range of 2.0 – 2.35, substantially above the sooting limit of $\phi \approx 1.8$ [18] and exit velocities ranging from $v$ = 5.3 to 13.6 cm/s, resulting in temperature variations between 1600 and 1850 K. Here, LII is used to measure soot volume fractions, while angle-dependent light scattering (ADLS) is used as a less-invasive alternative to ex situ methods such as TEM to measure the aggregates' radii of gyration. The experimental results are compared with numerical simulations using semiempirical two-equation models of soot formation by Leung et al. [19] and by Liu et al. [20]. Although more detailed models exist, these two-equation models are widely applied in numerical studies on soot formation because of their relatively low computational cost and reasonable accuracy for the flame conditions for which they have been derived [21–24].

## 2. Experimental Setup

*2.1. Burner System and Gas Supply.* Soot aggregates were produced in flat, premixed ethylene/air flames at atmospheric pressure. The flames were stabilized above a 60-mm diameter water-cooled McKenna burner and nitrogen was passed through the outer shroud ring to suppress flame instabilities and to prevent mixing with ambient air. Note that no stabilization plate or chimney was used in these experiments to limit the number of control parameters compared to other studies [25], using only the nitrogen shroud to stabilize the flame as suggested by Gothaniya et al. [17]. Flame stability was judged both by eye, and based on the stability of the LII and light scattering signal, measurements were only performed for conditions when there was no obvious wavering or flickering of the flame and if the signal was stable without periodic fluctuations. The axial distance between the measuring volume and the vertically mounted burner surface (HAB) was varied by moving the burner, which is mounted on a positioner (Parker), in 1 or 2 mm increments. In the present study the flame temperature was varied by changing the mass flux of the fuel/air mixture through the burner, which determines the degree of stabilization and thereby the amount of heat transferred to the burner [26, 27], allowing variation of the flame temperature at fixed $\phi$. It should be pointed out that in 1D burner-stabilized flames the upstream heat losses and herewith the flame temperature is completely determined by the velocity of the unburned fuel/air mixture. Therefore, measuring heat losses into the burner deck is not required in this experimental setup to derive the flame temperature. Flames with the desired fuel equivalence ratio and temperature were obtained by setting appropriate ethylene and air flow rates using the gas flow control and measurement system described in [28]. To improve accuracy and reproducibility, the gas flow rates set by Alicat MC-series mass flow controllers were also measured by Bronkhorst Hi-Tec EL-FLOW meters. Differences between the measured and set values of flows were less than 2% in the working range from 9 to 22 SLPM (298 K, 1 atm).

*2.2. Raman Temperature Measurements.* Flame temperatures were measured by spontaneous Raman spectroscopy, using the setup and method described in [29], utilizing the Stokes vibrational bands of $N_2$, which are fairly well separated from the excitation laser line (~2300 $cm^{-1}$). For the experiments described here, deriving temperatures by fitting the acquired Raman spectra is complicated in progressively richer flames because it becomes increasingly difficult to distinguish the weak spontaneous Raman signal from the background signals from of soot radiation and Rayleigh scattering, which

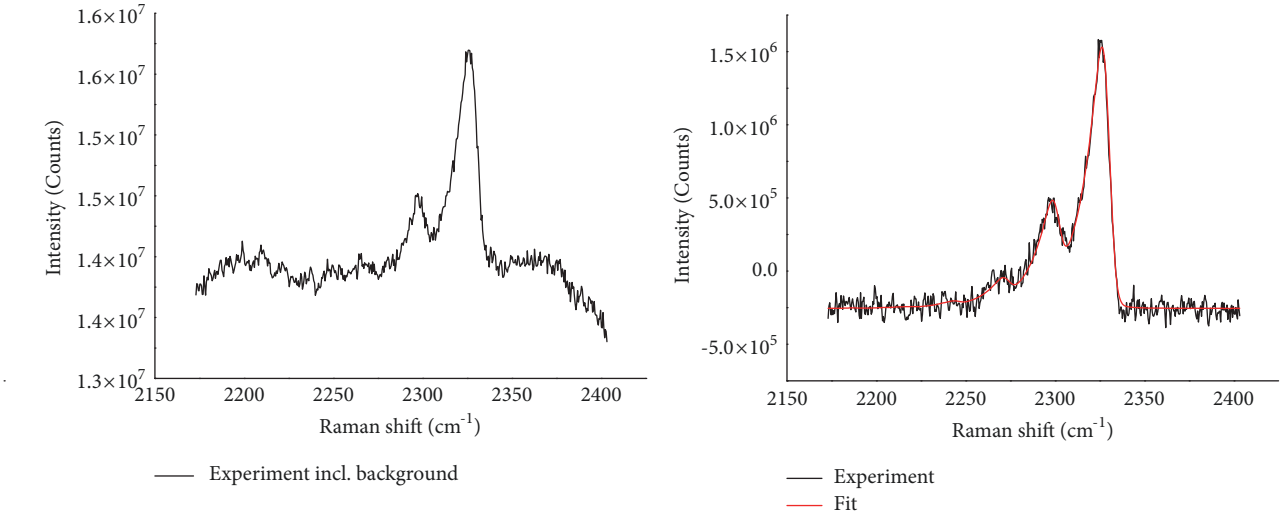


Figure 1: Spontaneous Raman spectrum of nitrogen in a rich ($\phi$ = 2.1) ethylene flame before (left) and after subtracting background (right) at HAB 5 mm for an exit velocity of 10 cm/s. Fitting yields a temperature of 1775 K.

is not completely eliminated by the filter/spectrometer combination. Raman thermometry could be used to determine temperatures of flames with equivalence ratios up to about $\phi$ = 2.1, depending on the exit velocity of the ethylene/air mixture. The Raman signal was always measured twice, once with the laser beam polarized perpendicular to the scattering plane and once with parallel polarization, using a half-wave plate to rotate the polarization. Because the background signal is unpolarized, it can be significantly reduced by subtracting the signal measured with parallel incident radiation from the signal with perpendicular incident radiation. However, since the measurements with different polarization of the incident beam are not performed simultaneously, this background subtraction procedure does not eliminate noise. For this reason, excessive levels of noise at high soot concentration limit the range of flame conditions where temperatures can be measured. Additionally, the increase in background necessitated shorter acquisition times before reading out the signal to avoid overexposure of the CCD sensor. Hence a larger number of accumulations were required to obtain the same total exposure time as that for measurements in nonsooting flames, increasing the total measurement time substantially. A typical Raman spectrum measured at HAB 5 mm in a sooting flame with $\phi$ = 2.1 and exit velocity 10 cm/s is shown in Figure 1, before and after subtracting the background. The background under these conditions is roughly ten times higher than the Raman signal but can be eliminated quite effectively by the subtraction procedure. The fit for the resulting spectrum gives a temperature of 1775 K for this flame.

*2.3. Soot Measurements.* In this paper, we use LII, laser light extinction, and ADLS for measuring soot parameters in flames. The optical setup is shown in Figure 2. Soot volume fractions were derived from the peak of the measured LII signal. We used a Quanta Ray GCR-150 laser operated at 1064 nm and frequency of 25 Hz with a pulse width of 8 ns and energy of 70 mJ/pulse. The laser beam is focused by a 500 mm focal length lens above the center of the burner. The IR wavelength of the laser prevents generation of LIF signal from polycyclic aromatic hydrocarbons (PAHs) that might interfere with the measurements [30]. The LII signal is collected by a UV-Nikkor 105 mm f/4.5 lens placed perpendicular to the laser beam and detected by the photomultiplier (EMI 9558B) with a bandpass interference filter (wavelength 450 nm, bandwidth 40±8 nm, and Melles Griot 03 FIV 028) installed in front of it. The photomultiplier signal is measured by a 54830 series Infiniium Oscilloscope, averaging over 250 laser pulses for each measurement. Provided that all particles reach the same peak temperature (at the sublimation point), the peak signal in the Rayleigh approximation will be proportional to the volume fraction of the particles [31].

The LII measurements were calibrated in a $\phi$ = 2.2 ethylene flame with exit velocity of 8.8 cm/s at HAB 10 mm by measuring extinction (see Figure 2) of a 532 nm cw laser beam (Coherent Sapphire 100 mW laser). Under these conditions, we measured a decrease in laser power of ~4% after passing the burner, which gives $f_v$ = 0.074 ppm, assuming a value of 1.57-0.56$i$ for the refractive index of soot [32]. Additional measurements in other flames at various heights above the burner confirmed linear dependence of the LII signal on soot volume fraction in the range where light extinction measurements could be trusted to yield accurate results.

The measurements of particle size in the postflame zone were performed by laser light scattering, as described in our previous study [33]; the setup is also shown in Figure 2. In short, a laser beam is directed through the flame, and scattered light is detected at four different angles, $\theta$. As described previously [28], the radius of gyration is related to the angle-dependence of the scattered light intensity according to

$$\frac{I(0)}{I(\theta)} \approx 1 + \frac{1}{3}\left[\frac{4\pi}{\lambda}\sin\left(\frac{\theta}{2}\right)\right]^2 R_g^2 \quad (1)$$

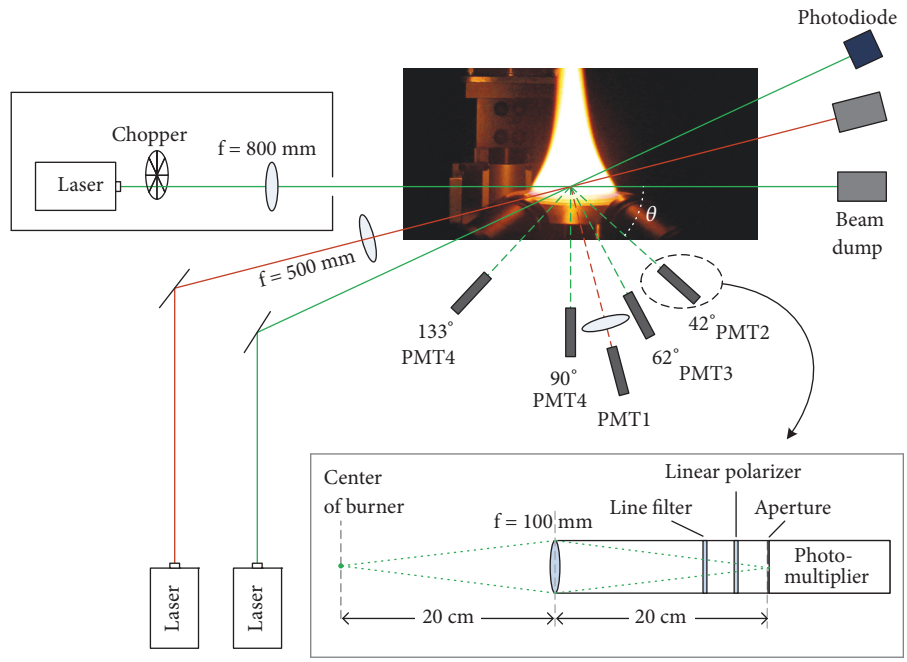


FIGURE 2: Schematic for the LII, extinction, and ADLS experimental setup. The LII signal is collected by photomultiplier PMT1. Angular orientations of the collection systems PMT2–PMT5 for ADLS measurements are denoted with respect to the forward direction of the laser beam.

where $I$ is the scattered light intensity. So, by plotting $1/I(\theta)$ as a function of $[(4\pi/\lambda)\sin(\theta/2)]^2$, the slope and intersection with y-axis of a linear fit can provide $R_g$. The limited sensitivity of the method resulted in a minimum measurement height of ~6 mm above the burner, depending on the equivalence ratio and exit velocity of the unburned gas mixture.

## 3. Flame Modeling

The numerical model used in this work is described in detail by Zimmer et al. [34], who assessed its accuracy for counterflow ethylene flames. The model consists of a set of one-dimensional conservation equations of mass, species mass, momentum, and energy. Diffusion is modeled using the Hirschfelder-Curtiss approximation [35] and the gas-phase reaction kinetics are modeled using the San Diego mechanism [36]. Soot formation and growth are based on the models by Leung et al. [19] and by Liu et al. [20], which are semiempirical acetylene based models that describe soot particle nucleation, surface growth, coagulation, and oxidation. Assuming a monodisperse soot particle distribution, the set of conservation equations is augmented by two conservation equations for soot mass fraction $Y_s$ and number density $N_s$ (in particles per kg of mixture), respectively. The mass and energy coupling of soot and gas-phase species as described in [34] is neglected because the soot mass fractions are sufficiently low in the present flames. The soot model of Liu et al. is a modified version of Leung et al., adding soot oxidation by OH and O (in addition to oxidation by $O_2$) and neglecting soot particle coagulation [20].

Premixed burner-stabilized flames are simulated by prescribing a mass flux and a fixed inlet temperature ($T = 300$ K), solving the energy equation in the rest of the domain. Gas and soot radiation are modeled using an optically thin grey-gas model with Planck mean absorption coefficients [34]. Since self-absorption of radiation is neglected, the heat loss can be overestimated. For the present flames, with a path length of about 5 cm, the radiative heat loss is 70% of the optically thin limit [37]. The soot volume fraction is calculated from the computed soot mass fraction as $f_v = \rho Y_s/\rho_s$, where $\rho_s$ is the density of soot (taken to be 2.0 g/cm$^3$ and 1.9 g/cm$^3$ in the models by Leung et al. and Liu et al. respectively [19, 34]).

## 4. Results and Discussion

*4.1. Temperature Measurements.* Measured temperatures for $\phi = 1.8$ and 2.0 and $v = 8.8$ cm/s are shown as function of HAB in Figure 3 and compared to calculations including and excluding radiative heat losses from the hot gases and soot. The maximum equivalence ratio for which such a vertical profile could be measured was $\phi = 2.0$. We note that the computations without radiative losses show superadiabatic temperatures close to the burner surface, which has been reported previously in rich hydrocarbon flames [38]. As can be seen, the measured flame temperature decreases with increasing axial distance (hence, increasing residence time), although not quite as strongly as predicted by the models. Given the impact of radiative losses on the temperature profiles illustrated by the computations, soot formation under these conditions is not an isothermal process, and caution should be exercised when characterizing the influence of

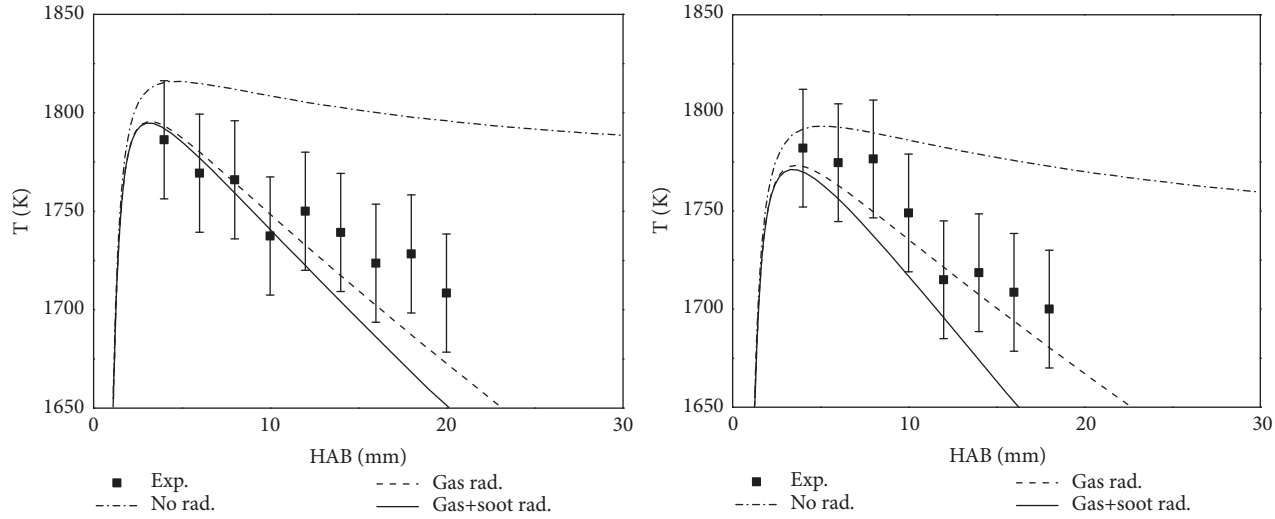


FIGURE 3: Comparison of flame temperatures for $\phi = 1.8$ (left) and 2.0 (right) at exit velocity $v = 8.8$ cm/s.

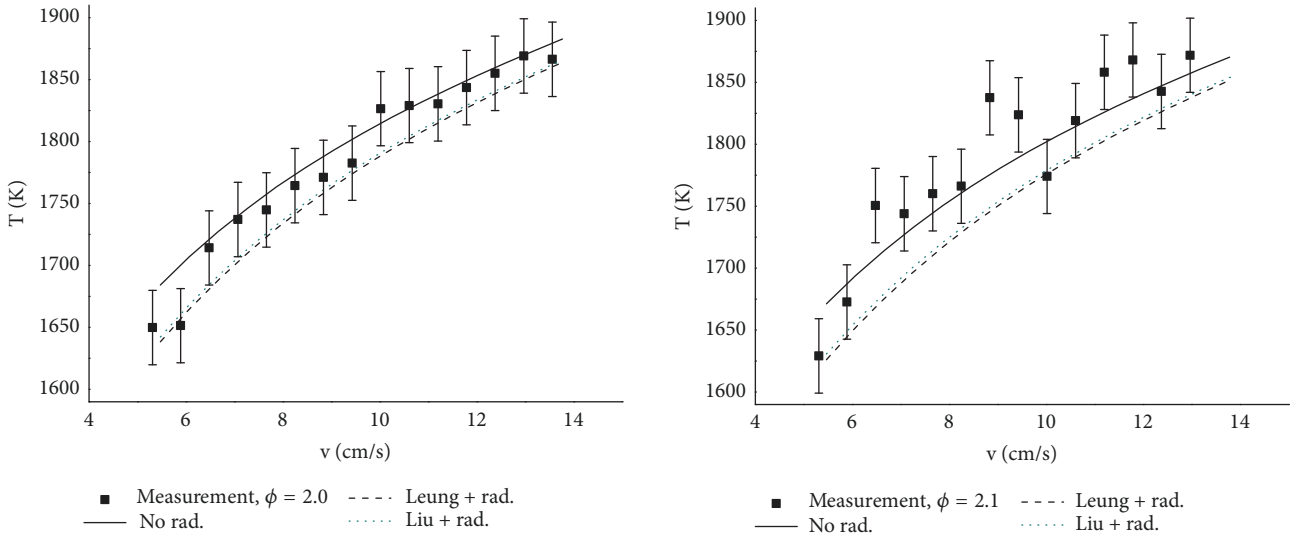


FIGURE 4: Comparison of calculated (with and without radiative heat losses) and measured flame temperatures for $\varphi = 2.0$ and $\phi = 2.1$ as a function of exit velocity at HAB = 5 mm.

temperature on soot formation in 1D flames. However, for the flames investigated here, the flame temperatures at HAB = 5 mm are within 30 K of those calculated without radiative losses; this is not unreasonable since at this distance heat release is essentially complete and the radiative losses are not yet substantial. As a result, we characterize the temperature variation at fixed $\phi$ by the temperature at HAB = 5 mm. We note that, despite the increased radiative heat transfer from soot at $\phi = 2.0$, there is little difference between the measured temperatures at the two equivalence ratios in Figure 3.

A comparison between measured and calculated flame temperatures for $\phi = 2.0$ and $\phi = 2.1$ at low HAB (5 mm) as a function of exit velocity, presented in Figure 4, shows that the computations continue to predict the temperature at this HAB well. Despite the scatter in the measurements in these sooting flames, the results suggest that the model may slightly overpredict the impact of radiative losses at 5 mm axial distance. Changing the exit velocity of the unburned fuel-air mixture from 5 to 14 cm/s results in a temperature variation in the range from roughly 1630 to 1850 K for $\phi = 2.1$. As indicated in Figure 3, the presence of a substantial density of soot precluded measurement in richer flames or at higher HAB where the impact of radiative heat losses is expected to be more significant. However, given the faithful reproduction of the measured temperatures as a function of equivalence ratio and mass flux, we will use the *computed* temperatures at HAB = 5 mm for all the flames studied to characterize the temperature variation in the analysis in Figure 4. This temperature is representative for especially the early stages of soot growth, but even for the richest flames in this work, heat losses will not affect the flame temperature too much until considerably higher HAB.

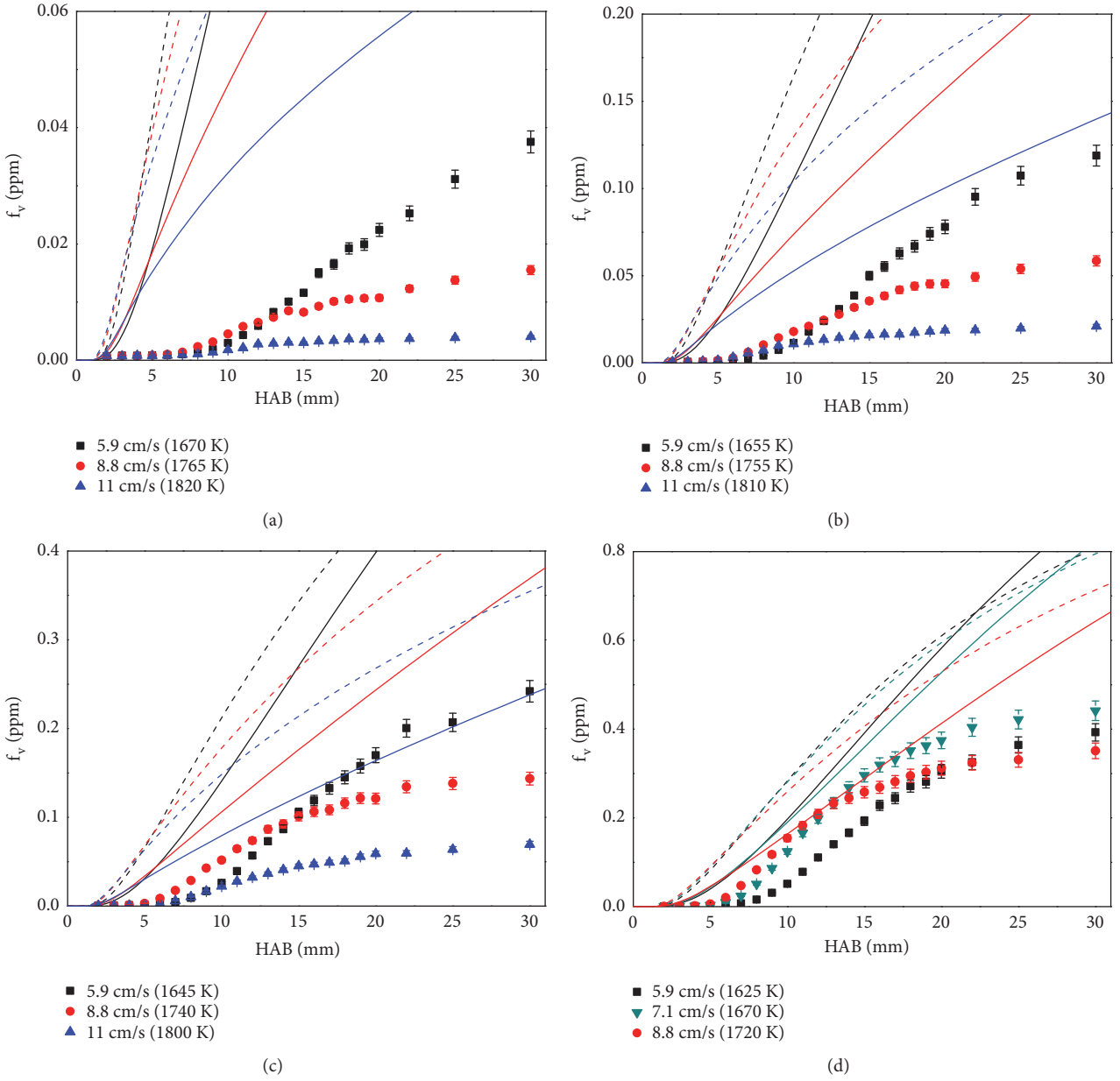


FIGURE 5: Comparison of $f_v$ results for three different exit velocities (symbols) and calculations using the models by Leung et al. [19] (dashed lines) and Liu et al. [20] (solid lines) at equivalence ratios (a) $\phi = 2.0$, (b) $\phi = 2.1$, (c) $\phi = 2.2$, and (d) $\phi = 2.35$.

*4.2. Soot Volume Fraction Measurements.* Axial profiles of measured and calculated soot volume fractions at $\phi = 2.0$, 2.1, 2.2, and 2.35 are presented in Figure 5 for representative exit velocities $v = 5.9$, 7.1, 8.8, and 11 cm/s (we remark that the flame at 11 cm/s and $\phi = 2.35$ was too unstable for reliable measurement). The error bars are based on the day-to-day reproducibility, which was within 10%. As can be seen, the soot volume fraction increases in all flames with the distance above the burner. At fixed distance, the soot volume fraction increases with increasing equivalence ratio.

In Figure 6 we compare $f_v$ for $\phi = 2.2$ at HAB = 30 mm as function of temperature (calculated at 5 mm) to final soot volume fractions $f_v\infty$ measured in a similar flame ($\phi = 2.16$) by Böhm et al. [8]. These results show excellent correspondence between the soot volume fractions obtained here using calibrated LII and those from extinction measurements in [8]. The agreement in the location of the maximum volume fraction as a function of temperature (see Figure 6) is also excellent. This agreement gives us additional confidence in the veracity of the measurements reported here.

Returning to Figure 5, we observe that the numerical calculations using both mechanisms of soot formation over-predict the measured volume fractions substantially. For example, measured maximum soot concentrations in flames with $\phi = 2.0$, 2.1, 2.2, and 2.35 are 0.04, 0.1, 0.25, and 0.45 ppm, respectively, while the values calculated using the

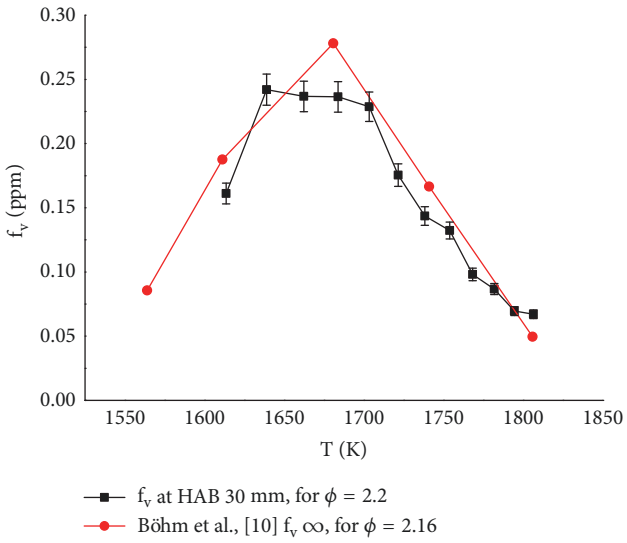


FIGURE 6: $f_v$ for $\phi = 2.2$ at HAB 30 mm as function of temperature (calculated at HAB 5 mm) to final soot volume fractions $f_v\infty$ measured in a similar flame ($\phi = 2.16$) by Böhm et al. [8].

mechanism of Liu et al. [20] are 0.3, 0.4, 0.60, and 0.8 ppm for the same flame conditions. Liu's model, which as described above has slightly more chemical detail, has somewhat better agreement with the measurements. The earlier onset of soot formation in the models compared to the measurements is probably because the soot models assume $C_2H_2$ as a direct soot precursor. Polycyclic aromatic hydrocarbons (PAHs), which have been observed to appear downstream of the acetylene peak but upstream of the rise in soot volume fraction [6], were found to play a more important role in soot growth in premixed $C_2H_4$/air flames [39]. We expect a more detailed treatment of soot formation to improve this shortcoming. Lastly, we comment that the improved agreement between model predictions and measurements with increasing equivalence ratio is rather to be expected, since the models were optimized for nonpremixed counterflow flames in which much higher soot fractions were observed. The semiempirical models used here lack the physical basis to be applied generally without parameter tuning.

To facilitate the further analysis, a comprehensive overview of the measurements and calculations of soot volume fraction is shown as contour plots in Figure 7. In the contour plots, vertical cross sections show axial profiles at fixed exit velocity, while horizontal cross sections represent the dependence of $f_v$ upon exit velocity at fixed HAB. Only contour plots of the calculations using the model of Liu et al. [20] model are shown, because of their slightly better agreement with the measurements.

We first remark that the calculations using the Liu model yielded maximum soot volume fractions at lower exit velocities than the minimum exit velocity studied in the experiments. Given the absence of soot oxidation paths in these very fuel-rich flames, we observe a steady increase in $f_v$ with increasing HAB, for all equivalence ratios and exit velocities, as illustrated in Figure 5. Also, referring to the legend accompanying the color scale, $f_v$ is seen to increase strongly with equivalence ratio, by roughly a factor of four when increasing $\phi$ from 2.1 to 2.35. More interesting is the nonmonotonic dependence of $f_v$ on exit velocity and thus on temperature at fixed height above the burner, initially increasing with exit velocity but decreasing at higher velocities. This behavior has been observed previously [6, 8] and was ascribed [6] to the temperature-dependent changes in PAH formation resulting in more or less soot inception, with lower temperatures (at low velocities) preventing PAHs from reacting to soot and higher temperatures (high velocities) oxidizing these species before they can contribute to soot formation. The observed trend of decreasing aggregate size at fixed HAB for high exit velocities is amplified by the decrease in residence time with exit velocity for any given HAB. It should be pointed out that the residence time is approximately inversely proportional to both the height above the burner and to the exit velocity. A change in either is accompanied by a change in flame temperature, but not to the degree that this has a strong bearing on the residence time. As can be seen in Figure 7 (and Figure 5), the maximum in the measured soot volume fraction occurs at temperatures around 1675 K for all equivalence ratios studied in this work, as observed in the other studies [6, 8]. The shift of the maximum in $f_v$ at fixed height above the burner to higher exit velocities in progressively richer flames is mostly due to the fact that in richer flames higher exit velocities are required to attain the same flame temperature.

*4.3. Aggregate Size Measurements.* With the current experimental setup, reliable ADLS measurements for a range of exit velocities could only be performed for flames with $\phi \geq 2.1$. At lower $\phi$, due to the small aggregate size, the signal differences between even the outermost PMTs are too small to detect them reliably. While the numerical models do not attempt to calculate the aggregate gyration radius, it is instructive to derive $R_g$ based on the simple consideration of spherical particles, calculating $R_g$ as $\sqrt{3/5}R$ with $R$ the radius of a soot particle, which is computed as $R = (3Y_s/4\pi\rho_s N_s)^{1/3}$. The radius of gyration derived thusly serves as a lower limit, since in actuality the aggregates are known to be less compact, with the typical fractal dimension of soot being ~1.8 [40]. Axial profiles of measured and calculated $R_g$ as function of HAB for a number of exit velocities are shown in Figure 8. The error bars are based on the quality of the least square fit used to derive $R_g$, with a minimum of at least the day-to-day reproducibility (always within 10%).

As observed for $f_v$, the measured soot radius of gyration increases with increasing HAB for all equivalence ratios and exit velocities. As expected, $R_g$ is substantially larger in richer flames: in the flames at $\phi = 2.35$ flames $R_g$ is roughly twice that for flames at $\phi = 2.1$. We note that early scattering measurements [41] for a flame within the range of temperature and equivalence ratio to those reported here ($\phi = 2.28$, flame temperature 1740 K) ultimately yielded averaged particle diameters of ~ 40 nm, whereas the particle diameters based on $R_g$ obtained using ADLS are estimated to be roughly 60 nm. We also observe that although the measured profiles

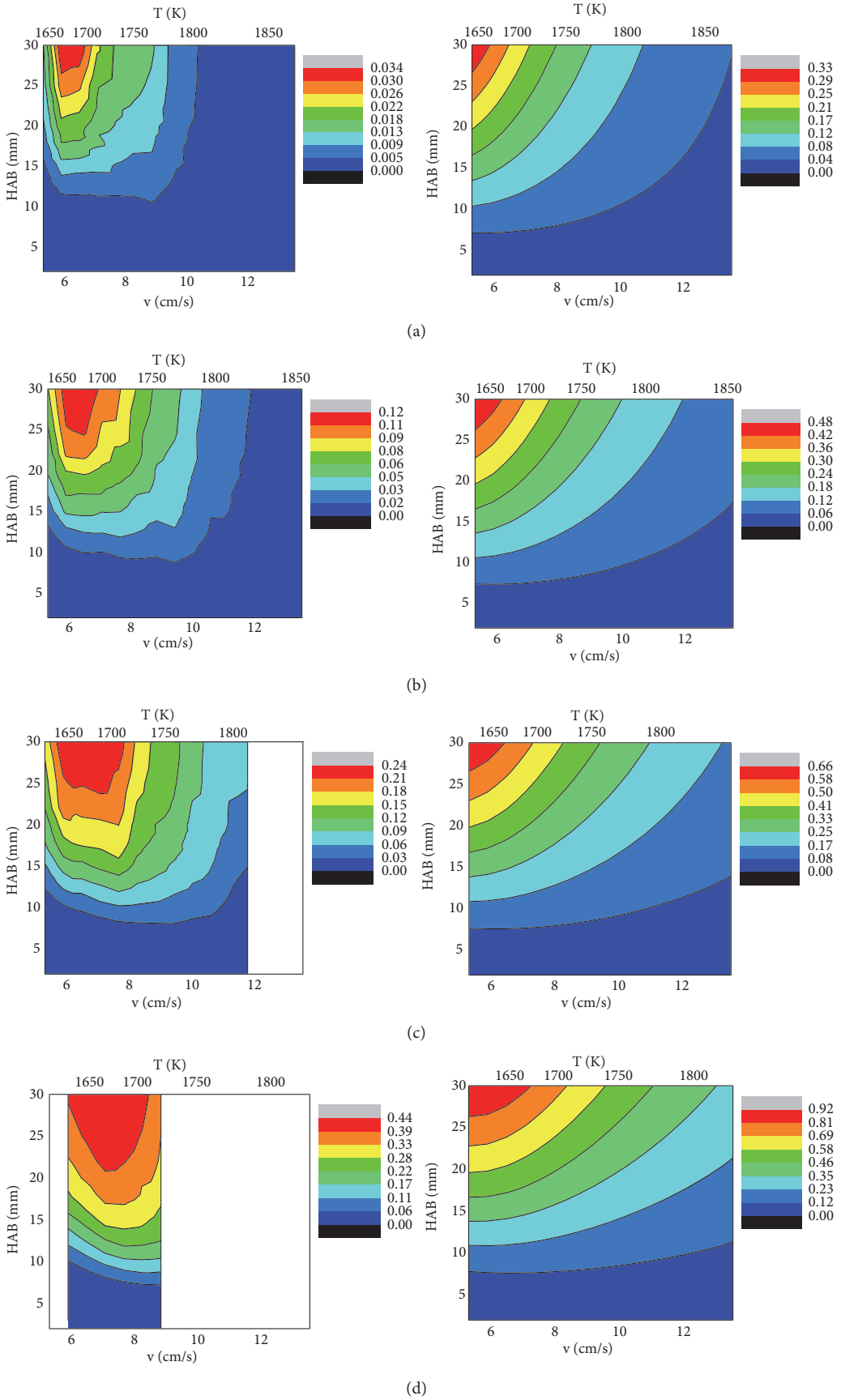


FIGURE 7: Contour plots of the measured (left) and calculated—using the Liu model—(right) soot volume fraction (ppm) as function of HAB and exit velocity $v$ for equivalence ratios (a) $\phi = 2.0$, (b) $\phi = 2.1$, (c) $\phi = 2.2$, and (d) $\phi = 2.35$.

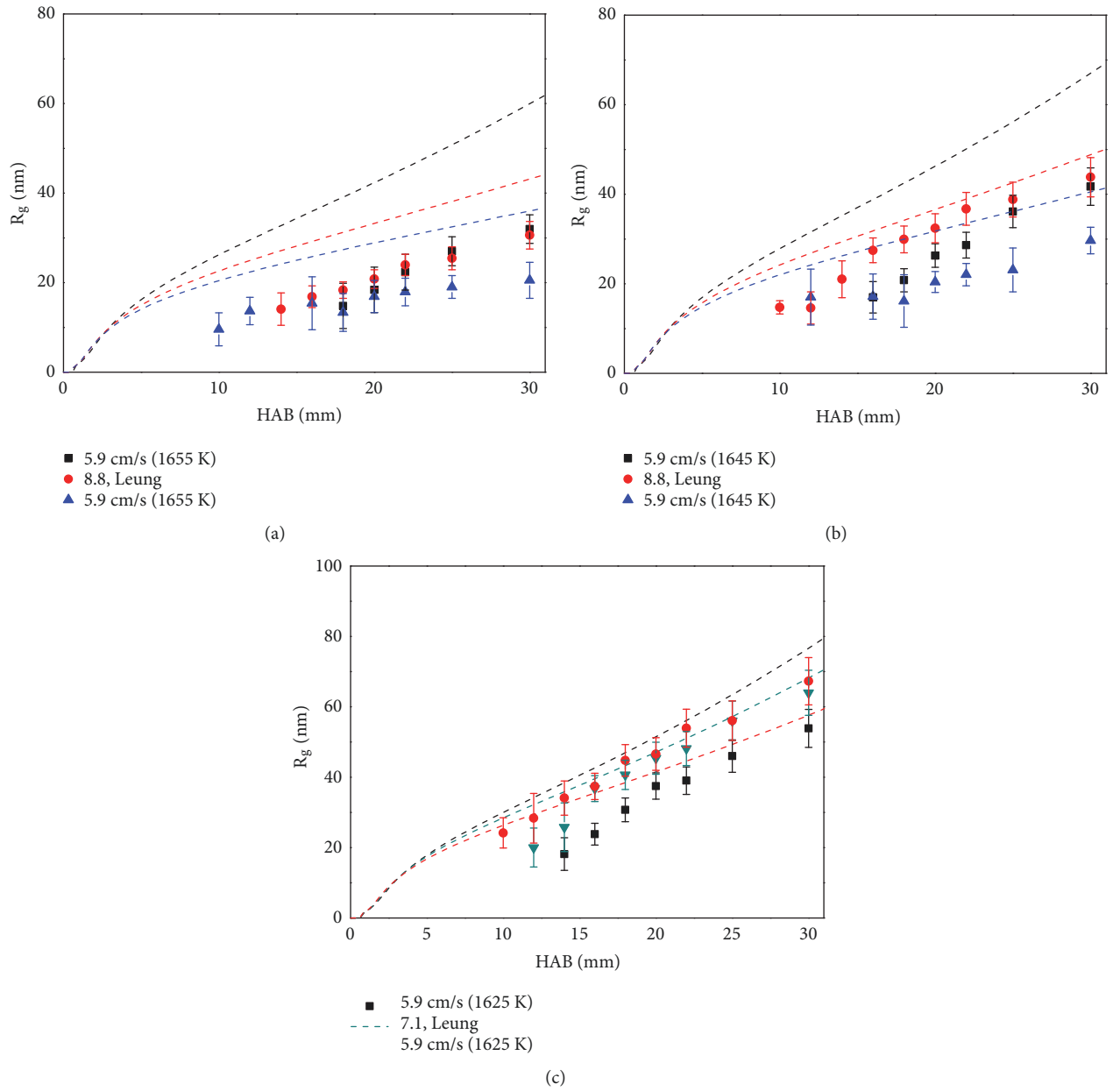


FIGURE 8: Measured (symbols) and computed (Leung et al. [19], dashed lines) axial profiles of $R_g$ for three different exit velocities at equivalence ratios (a) $\phi = 2.1$, (b) $\phi = 2.2$, and (c) $\phi = 2.35$.

of $f_v$ for the richer flames (Figures 5(c) and 5(d)) tend to flatten at higher HAB, the measured $R_g$ is still increasing, suggesting agglomeration as the dominant process at larger axial distances.

While the model of Liu et al. [20] showed somewhat better agreement for $f_v$ (see Figure 5, above) it lacks any physical basis for calculating $R_g$ because this model does not take account for coagulation of particles. Consequently, we only consider the model of Leung et al. [19]. From Figure 8, we observe that the numerical calculations using the model from Leung et al. [19] to predict the radii of gyration appear in reasonable agreement with the experimental results at higher equivalence ratio, despite the poorer prediction of soot volume fraction. However, as mentioned before, the calculated $R_g$ is based on the consideration of coagulation to spherical particles rather than agglomerates, which at best provides a lower estimate of particle size. Based on a typical fractal dimension of ~1.8 [40] and a monomer size of 10 nm [42] we can conclude that for the maximum height at $\phi = 2.35$ we underestimate the actual $R_g$ of an aggregate structure of equal mass by over a factor of three. This means that the calculated $R_g$ should have been much smaller for the model to be in reasonable agreement with the measurements.

The contour plots summarizing all the $R_g$ data are shown in Figure 9. The figures giving the experimental data show, to our knowledge, a hitherto unreported nonmonotonic

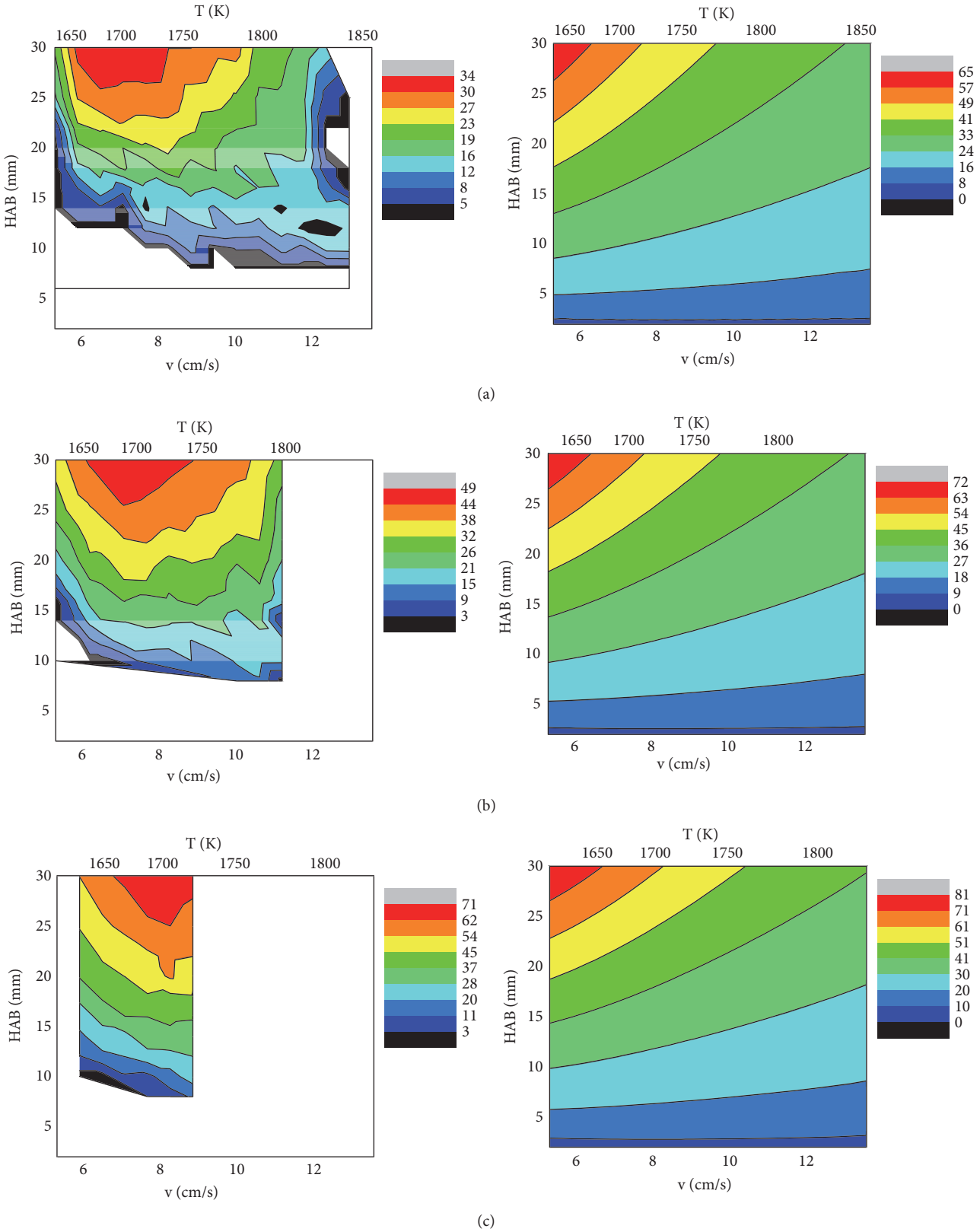


FIGURE 9: Contour plots of the measured (left) and calculated (right) radius of gyration (nm) as function of HAB and exit velocity $v$ for equivalence ratios (a) $\phi = 2.1$, (b) $\phi = 2.2$, and (c) $\phi = 2.35$. Only the computations using the model of Leung et al. [19] are shown (see text).

dependence of $R_g$ on exit velocity/flame temperature as is observed for $f_v$, (see Figure 7).

Here too, we observe the shift of the maximum to higher exit velocities with increasing equivalence ratio. However, analogous to the volume fraction, the maximum radius of gyration also occurs at constant temperature, independent of equivalence ratio. The maximum $R_g$ occurs at higher exit velocities than $f_v$, corresponding to a flame temperature of roughly 1700 K. As is the case for the soot formation, the decrease in residence time for a given HAB with increasing exit velocity amplifies the observed trend of decreasing aggregate size at fixed HAB for high exit velocities. Similar to the behavior observed for the soot volume fraction, the computations show the peak $R_g$ at lower exit velocities than the experimental results.

## 5. Conclusions

The growth of soot volume and aggregate size was studied in 1D premixed fuel-rich ethylene/air flames for various equivalence ratios and a range of temperatures using laser-induced incandescence and angle-dependent light scattering to measure the soot volume fraction and radius of gyration, respectively. Flame temperatures derived from spontaneous Raman scattering in flames with equivalence ratios up to $\phi$ = 2.1 showed good correspondence to temperatures calculated using the San Diego mechanism.

Similar to previous studies [17], the LII measurements showed a substantial impact of the fuel equivalence ratio on the soot volume fraction, with $f_v$ at $\phi$ = 2.35 being over ten times as big as that at $\phi$ = 2.0. Furthermore, we observe a nonmonotonic dependence of the measured $f_v$ on the exit velocity of the fuel-air mixture, with an initial increase and later decrease for higher velocities. The maximum $f_v$ shifts to higher exit velocities in progressively richer flames. However, the maximum $f_v$ occurs at a flame temperature of around 1675 K, regardless of equivalence ratio.

We also observed a strong impact of $\phi$ on the radius of gyration $R_g$ of the generated soot particles, with particles formed at $\phi$ = 2.35 having a radius roughly twice as big as those formed at $\phi$ = 2.1. Furthermore, we observe a similar dependence on the fuel-air exit velocity as $f_v$, with the maximum at somewhat higher velocities, i.e., at a slightly higher flame temperature of around 1700 K. The use of a laser with shorter wavelength should enable extension of these measurements to lower equivalence ratios in the future.

The measurement results were compared with calculations using semiempirical two-equation models of soot formation by Leung et al. [19] and by Liu et al. [20]. The models do relatively well predicting $f_v$ in richer flames, Liu et al. yielding slightly better agreement for all conditions, but calculations using both mechanisms substantially overpredict the measured volume fractions. For predicting $R_g$, Liu's model is inherently unsuitable because it does not take coagulation into account. Leung's model does consider coagulation but is limited as it only assumes spherical particles, rather than more detailed (and more correct) particle morphology. Like for $f_v$, the agreement between the experimental results and predictions of the numerical simulations using Leung's model is better in richer flames, but based on simple consideration of typical fractal dimension and monomer size the simulations still overpredict the measured radii of gyration substantially. Future research will compare the results reported here with a more detailed model.

## Data Availability

The experimental and calculated results associated with this article can be found in the supplementary material.

## Conflicts of Interest

The authors declare that they have no conflicts of interest.

## Supplementary Materials

The experimental and calculated results associated with this article can be found in the supplementary material. *(Supplementary Materials)*

## References

[1] J. Kolosnjaj-Tabi, J. Just, K. B. Hartman et al., "Anthropogenic Carbon Nanotubes Found in the Airways of Parisian Children," *EBioMedicine*, vol. 2, no. 11, pp. 1697–1704, 2015.

[2] H. Wang, "Formation of nascent soot and other condensed-phase materials in flames," *Proceedings of the Combustion Institute*, vol. 33, no. 1, pp. 41–67, 2011.

[3] S. Will, S. Schraml, and A. Leipertz, "Two-dimensional soot-particle sizing by time-resolved laser-induced incandescence," *Optics Expresss*, vol. 20, no. 22, pp. 2342–2344, 1995.

[4] S. Will, S. Schraml, and A. Leipert, "Comprehensive two-dimensional soot diagnostics based on laser-induced incandescence (LII)," *Symposium (International) on Combustion*, vol. 26, no. 2, pp. 2277–2284, 1996.

[5] J. Reimann, S. Kuhlmann, and S. Will, "2D aggregate sizing by combining laser-induced incandescence (LII) and elastic light scattering (ELS)," *Applied Physics B: Lasers and Optics*, vol. 96, no. 4, pp. 583–592, 2009.

[6] A. Ciajolo, A. D'anna, R. Barbella, A. Tregrossi, and A. Violi, "The effect of temperature on soot inception in premixed ethylene flames," *Symposium (International) on Combustion*, vol. 26, no. 2, pp. 2327–2333, 1996.

[7] C. Gu, H. Lin, J. Camacho et al., "Particle size distribution of nascent soot in lightly and heavily sooting premixed ethylene flames," *Combustion and Flame*, vol. 165, pp. 177–187, 2016.

[8] H. Böhm, D. Hesse, H. Jander et al., "The influence of pressure and temperature on soot formation in premixed flames," *Symposium (International) on Combustion*, vol. 22, no. 1, pp. 403–411, 1989.

[9] M. Bönig, C. Feldermann, H. Jander, B. Lüers, G. Rudolph, and H. G. Wagner, "Soot formation in premixed C2H4 flat flames at elevated pressure," *Symposium (International) on Combustion*, vol. 23, no. 1, pp. 1581–1587, 1991.

[10] P. Chambrion, H. Jander, N. Petereit, and H. G. Wagner, " Soot Growth in Atmospheric C ," *Zeitschrift für Physikalische Chemie*, vol. 194, no. Part_1, pp. 1–19, 1996.

[11] H. Mätzing and H. G. Wagner, "Measurements about the influence of pressure on carbon formation in premixed laminar

C2H4-air flames," *Symposium (International) on Combustion*, vol. 21, no. 1, pp. 1047–1055, 1988.

[12] F. Xu, P. B. Sunderland, and G. M. Faeth, "Soot formation in laminar premixed ethylene/air flames at atmospheric pressure," *Combustion and Flame*, vol. 108, no. 4, pp. 471–493, 1997.

[13] S. J. Harris and A. M. Weiner, "Determination of the Rate Constant for Soot Surface Growth," *Combustion Science and Technology*, vol. 32, no. 5-6, pp. 267–275, 2007.

[14] S. Harris and A. Weiner, "Surface Growth of Soot Particles in Premixed Ethylene/Air Flames," *Combustion Science and Technology*, vol. 31, no. 3-4, pp. 155–167, 1983.

[15] F. Carbone, K. Gleason, and A. Gomez, "Probing gas-to-particle transition in a moderately sooting atmospheric pressure ethylene/air laminar premixed flame. Part I: gas phase and soot ensemble characterization," *Combustion and Flame*, vol. 181, pp. 315–328, 2017.

[16] F. Carbone, S. Moslih, and A. Gomez, "Probing gas-to-particle transition in a moderately sooting atmospheric pressure ethylene/air laminar premixed flame. Part II: Molecular clusters and nascent soot particle size distributions," *Combustion and Flame*, vol. 181, pp. 329–341, 2017.

[17] G. Gothaniya, S. Lee, A. Menon, S. Iyer, J. Milton, and T. A. Litzinger, "A study on the effect of experimental setup configuration on soot formation in a laminar premixed ethylene-air flame," in *Combust. Gener. Fine Carbonaceous Part*, H. Bockhorn, A. DAnna, A. F. Sarofim, and H. Wang, Eds., Proc. an Int. Work. Held Villa Orlandi, pp. 697–711, KIT Scientific Publishing, 2007.

[18] P.-E. Bengtsson and M. Aldén, "Soot particle measurements in premixed ethylene flames using a pulsed laser method," *Journal of Aerosol Science*, vol. 19, no. 7, pp. 959–962, 1988.

[19] K. M. Leung, R. P. Lindstedt, and W. P. Jones, "A simplified reaction mechanism for soot formation in nonpremixed flames," *Combustion and Flame*, vol. 87, no. 3-4, pp. 289–305, 1991.

[20] F. Liu, H. Guo, G. J. Smallwood, and M. El Hafi, "Effects of gas and soot radiation on soot formation in counterflow ethylene diffusion flames," *Journal of Quantitative Spectroscopy & Radiative Transfer*, vol. 84, no. 4, pp. 501–511, 2004.

[21] F. Liu, H. Guo, G. J. Smallwood, and Ö. L. Gülder, "Numerical modelling of soot formation and oxidation in laminar coflow non-smoking and smoking ethylene diffusion flames," *Combustion Theory and Modelling*, vol. 7, no. 2, pp. 301–315, 2003.

[22] V. Raj Mohan and D. C. Haworth, "Turbulence-chemistry interactions in a heavy-duty compression-ignition engine," *Proceedings of the Combustion Institute*, vol. 35, no. 3, pp. 3053–3060, 2015.

[23] K. M. Pang, N. Karvounis, J. H. Walther, and J. Schramm, "Numerical investigation of soot formation and oxidation processes under large two-stroke marine diesel engine-like conditions using integrated CFD-chemical kinetics," *Applied Energy*, vol. 169, pp. 874–887, 2016.

[24] S. P. Roy and D. C. Haworth, "A Systematic Comparison of Detailed Soot Models and Gas-Phase Chemical Mechanisms in Laminar Premixed Flames," *Combustion Science and Technology*, vol. 188, no. 7, pp. 1021–1053, 2016.

[25] A. S. Feitelberg, J. P. Longwell, and A. F. Sarofim, "Metal enhanced soot and PAH formation," *Combustion and Flame*, vol. 92, no. 3, pp. 241–253, 1993.

[26] A. V. Mokhov and H. B. Levinsky, "A LIF and cars investigation of upstream heat loss and flue-gas recirculation as NOx control strategies for laminar, premixed natural-gas/air flames," *Proceedings of the Combustion Institute*, vol. 28, no. 2, pp. 2467–2474, 2000.

[27] A. V. Sepman, A. V. Mokhov, and H. B. Levinsky, "Extending the predictions of chemical mechanisms for hydrogen combustion: Comparison of predicted and measured flame temperatures in burner-stabilized, 1-D flames," *International Journal of Hydrogen Energy*, vol. 36, no. 15, pp. 9298–9303, 2011.

[28] P. N. Langenkamp, A. V. Mokhov, and H. B. Levinsky, "Angle-Dependent Light Scattering Study of Silica Aggregate Growth in 1-D Methane/Air Flames with Hexamethyldisiloxane Admixture: Effects of Siloxane Concentration, Flame Temperature, and Equivalence Ratio," *Combustion Science and Technology*, vol. 189, no. 1, pp. 132–149, 2017.

[29] A. V. Sepman, V. V. Toro, A. V. Mokhov, and H. B. Levinsky, "Determination of temperature and concentrations of main components in flames by fitting measured Raman spectra," *Applied Physics B: Lasers and Optics*, vol. 112, no. 1, pp. 35–47, 2013.

[30] C. Schoemaecker Moreau, E. Therssen, X. Mercier, J. Pauwels, and P. Desgroux, "Two-color laser-induced incandescence and cavity ring-down spectroscopy for sensitive and quantitative imaging of soot and PAHs in flames," *Applied Physics B: Lasers and Optics*, vol. 78, no. 3-4, pp. 485–492, 2004.

[31] H. A. Michelsen, C. Schulz, G. J. Smallwood, and S. Will, "Laser-induced incandescence: Particulate diagnostics for combustion, atmospheric, and industrial applications," *Progress in Energy and Combustion Science*, vol. 51, pp. 2–48, 2015.

[32] K. C. Smyth and C. R. Shaddix, "The elusive history of m = 1.57 - 0.56i for the refractive index of soot," *Combustion and Flame*, vol. 107, no. 3, pp. 314–320, 1996.

[33] P. N. Langenkamp, H. B. Levinsky, and A. V. Mokhov, "The effects of hydrogen addition on silica aggregate growth in atmospheric-pressure, 1-D methane/air flames with hexamethyldisiloxane admixture," *International Journal of Hydrogen Energy*, vol. 43, no. 5, pp. 2997–3003, 2018.

[34] L. Zimmer, F. M. Pereira, J. A. van Oijen, and L. P. de Goey, "Investigation of mass and energy coupling between soot particles and gas species in modelling ethylene counterflow diffusion flames," *Combustion Theory and Modelling*, vol. 21, no. 2, pp. 358–379, 2017.

[35] J. Hirschfelder, C. Curtiss, and R. Bird, *Molecular theory of gases and liquids*, John Wiley Sons, Inc, New York, 1954.

[36] Chemical-Kinetic Mechanisms for Combustion Applications, San Diego Mechanism web page, Mechanical and Aerospace Engineering (Combustion Research), University of California at San Diego (http://combustion.ucsd.edu), December 2016.

[37] F. A. Lammers and L. P. H. De Goey, "The influence of gas radiation on the temperature decrease above a burner with a flat porous inert surface," *Combustion and Flame*, vol. 136, no. 4, pp. 533–547, 2004.

[38] F. Liu, H. Guo, G. J. Smallwood, and Ö. L. Gülder, "Numerical study of the superadiabatic flame temperature phenomenon in hydrocarbon premixed flames," *Proceedings of the Combustion Institute*, vol. 29, no. 2, pp. 1543–1550, 2002.

[39] T. G. Benish, A. L. Lafeur, K. Taghiadeh, and J. B. Howard, "C2H2 and PAH as soot growth reactants in premixed C2H4-air flames," *Symposium (International) on Combustion*, vol. 26, no. 2, pp. 2319–2326, 1996.

[40] C. M. Sorensen, "Light Scattering by Fractal Aggregates: A Review," *Aerosol Science and Technology*, vol. 35, no. 2, pp. 648–687, 2001.

[41] B. S. Haynes, H. Jander, and H. G. Wagner, "The effect of metal additives on the formation of soot in premixed flames," *Symposium (International) on Combustion*, vol. 17, no. 1, pp. 1365–1374, 1979.

[42] S. De Iuliis, S. Maffi, F. Migliorini, F. Cignoli, and G. Zizak, "Effect of hydrogen addition on soot formation in an ethylene/air premixed flame," *Applied Physics B: Lasers and Optics*, vol. 106, no. 3, pp. 707–715, 2012.

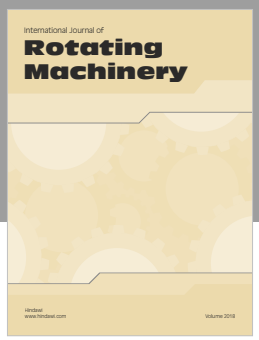

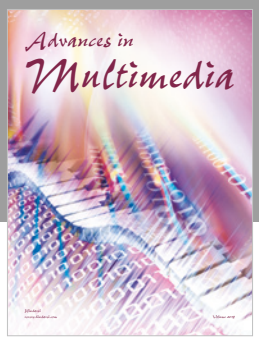

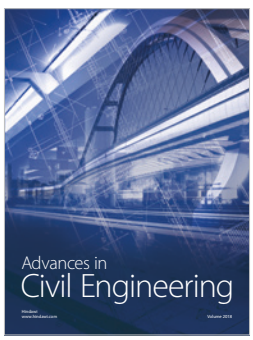

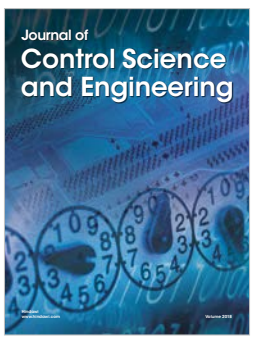

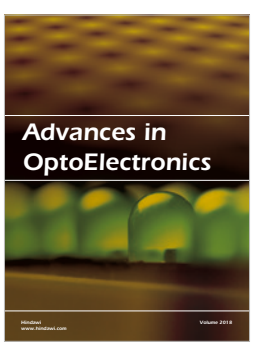

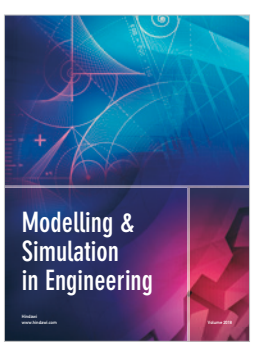

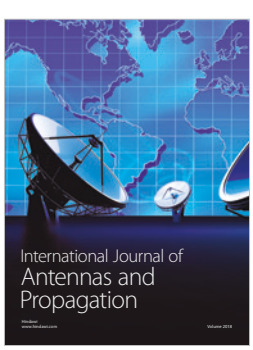

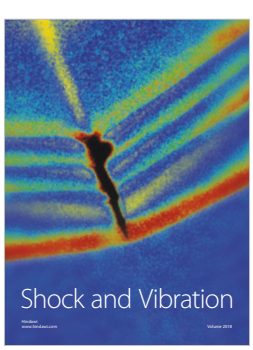

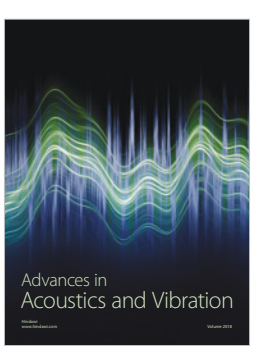

Hindawi

Submit your manuscripts at
www.hindawi.com